Quantum Transport through a Single Conjugated Rigid Molecule, a Mechanical Break Junction Study

Frisenda, Riccardo; Stefani, Davide; Van Der Zant, Herre S.J.

DOI
10.1021/acs.accounts.7b00493

Publication date
2018

Document Version
Final published version

Published in
Accounts of Chemical Research

ACCOUNTS of chemical research

Article

Cite This: Acc. Chem. Res. 2018, 51, 1359−1367

pubs.acs.org/accounts

Quantum Transport through a Single Conjugated Rigid Molecule, a Mechanical Break Junction Study

Riccardo Frisenda,*[,†,‡,∥] Davide Stefani,[†,∥] and Herre S. J. van der Zant*[,†,‡,§]

[†]Kavli Institute of Nanoscience, Delft University of Technology, Delft 2600 GA, The Netherlands

[‡]Instituto Madrileño de Estudios Avanzados de Nanociencia (IMDEA-nanociencia), E-28049 Madrid, Spain

[§]Departamento de Física de la Materia Condensada, Universidad Autónoma de Madrid, E-28049 Madrid, Spain

Supporting Information

CONSPECTUS: This Account provides an overview of our recent efforts to unravel charge transport characteristics of a metal−molecule−metal junction containing an individual π-conjugated molecule. The model system of our choice is an oligo(phenylene-ethynylene) consisting of three rings, in short OPE3, which represents a paradigmatic model system for molecular-scale electronics. Members of the OPE family are among the most studied in the field thanks to their simple and rigid structure, the possibility of chemically functionalizing them, and their clear transport characteristics. When investigating charge transport in molecular systems, two general directions can be distinguished: one in which assemblies composed of many molecules contacted in parallel are studied, while in the other a single molecule is investigated at a time. In the former approach, molecule−molecule interactions and ensemble-averaged quantities may play a role, thereby introducing broadening of spectral features and hindering the study of the behavior of individual molecules making it more difficult to deconvolute local and intrinsic molecular effects from collective ones. In contrast, single-molecule experiments directly probe individual molecular features and, when they are repeated many times, allow build up of a statistical representation of the changes introduced by, e.g., different junction configurations. Especially in recent years, experimental techniques have advanced such that now large sets of individual events can be measured and analyzed with statistical tools. To study individual single-molecule junctions, we use the break junction technique, in which two sharp movable electrodes are formed by breaking a thin metallic wire and used to contact a single or few molecules. By probing thousands of single-molecule junctions in different conditions, we show that their creation involves independent events justifying the statistical tools that are used. By combining room- and low-temperature data, we show that the dominant transport mechanism for electrons through the OPE3 molecule is off-resonant tunneling. The simplest model capturing transport details in this case is a single-level model characterized by three parameters: the level alignment of the frontier orbital with the Fermi energy of the leads and the electronic couplings to the leads. Variations in these parameters give a broad distribution (1 order of magnitude) in the observed conductance values, indicating that at the microscopic level both the hybridization with the metallic electrodes and the molecular electronic configuration can fluctuate. The low-temperature data show that these variations are due to abrupt changes in the configuration of the molecule in the junction leading to changes in either one of these parameters or both at the same time. The complementary information gained from different experiments is needed to build up a consistent and extended picture of the variability of molecular configurations, omnipresent in single-molecule studies. Knowledge of this variability can help one to better understand the behavior of molecules at the atomic level and at the metal−molecule interface in particular.

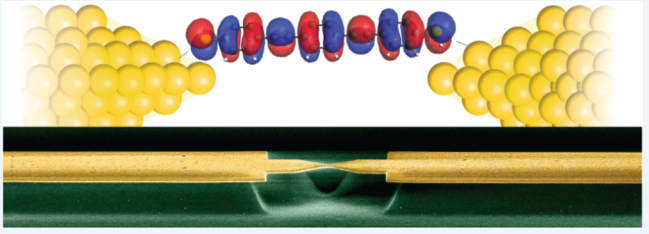

I. INTRODUCTION

Molecular-scale electronics studies the electrical properties of molecules with the aim to better understand the fundamental transport aspects and the potential applications in electronics.[1−3] A popular technique to electrically contact a single molecule encompasses break junctions, of which there are two main types: one is based on scanning probe microscopy[4,5] (SPM), while in the other, the mechanically controlled break junction technique (MCBJ), a thin metallic wire is broken by applying mechanical stress to it (Figure 1a−c). A priori it is not clear that the two approaches would yield the same conductance properties: in the SPM approach,[6] one electrode is a flat metallic surface and the other a sharp tip; whereas in the MCBJ technique,[7] two sharp tips are used. Consequently, the dynamics of junction formation and the conformation of the molecule in the junction can be different, leading to different junction formation yields or conformations. Compared to SPM the MCBJ technique has the advantage of larger mechanical stability, yielding junction lifetimes of many hours even at room temperature. At present, only for a few molecules measurements in both platforms have been reported: the molecule under consideration here is one of them.[8−10] We further note that there are other platforms capable of measuring electrical

Received: October 2, 2017
Published: June 4, 2018

DOI: 10.1021/acs.accounts.7b00493
Acc. Chem. Res. 2018, 51, 1359−1367

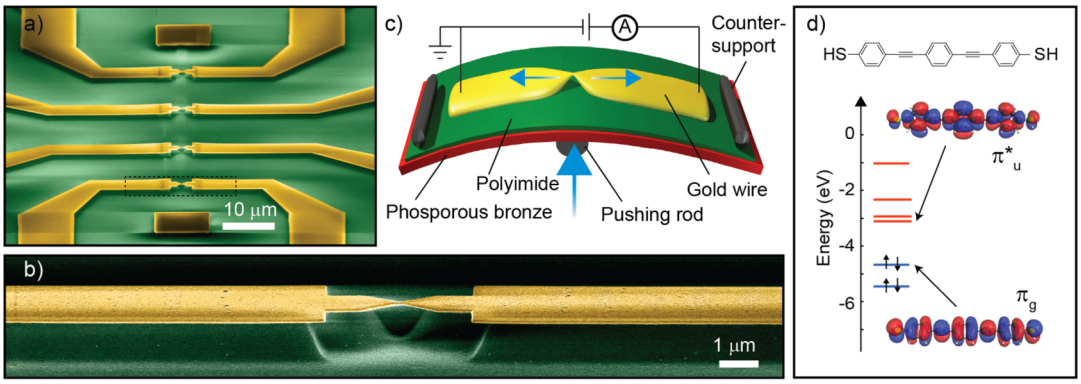

Figure 1. (a) Scanning electron microscopy images of four parallel wires of a MCBJ sample and (b) of the central constriction of one of the wires. (c) Scheme of the MCBJ setup. (d) Chemical drawing of an OPE3 molecule and electronic structure in gas phase calculated with DFT B3LYP//TZ2P.

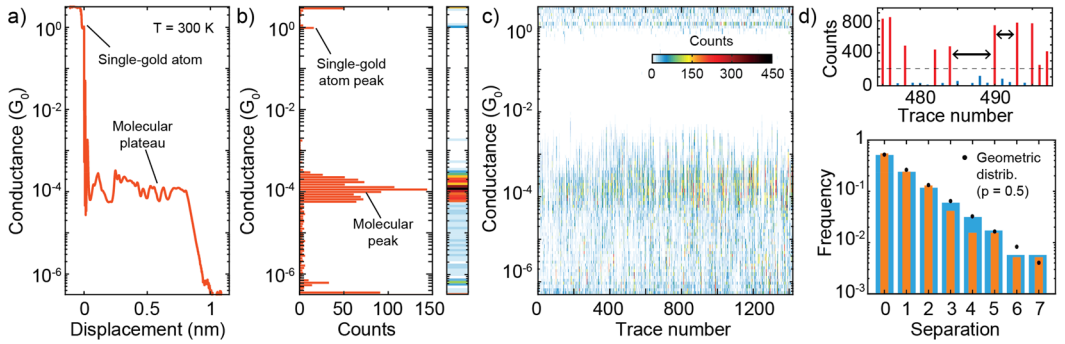

Figure 2. (a) Conductance−displacement trace measured in the presence of OPE3 at room temperature, bias 0.1 V, and speed 5 nm/s. (b) Histogram built from the trace in (a) by logarithmically binning the conductance. Right: histogram represented as a color map. (c) Two-dimensional color map built from 1450 breaking traces of OPE3 color-coded like in (b). (d) Histograms built from trace number 25 to 725 (blue) and from 725 to 1425 (orange) by counting the number of empty junctions traces separating two subsequent molecular junctions (bottom). The black dots represent a geometric distribution with probability $p = 0.5$.

transport through single molecules, such as electromigration of metallic wires or nanogaps in graphene.[3]

In this Account, we discuss MCBJ experiments on a rigid and π-conjugated oligo(phenelyne-ethynylene) derivative with three benzene rings, OPE3 in short. At either end, acetyl-protected thiol groups provide the anchoring to the electrodes (Figure 1d). OPE3 has a relatively high conductance and forms stable and well-distinguishable molecular features in MCBJ experiments.[11−23] These characteristics make it a "fruit fly" molecule for detailed single-molecule transport studies and for statistical analysis of single-molecule traces. Special attention will be paid to those experimental approaches that exploit the stability and the control over the electrodes separation of the MCBJ technique. Importantly, the technique also allows measurements at different temperatures, and here we discuss a comparison between room-temperature and low-temperature experiments at 6 K.[22]

II. FABRICATION AND MEASUREMENT TECHNIQUES

MCBJ samples (see Figure 1a,b) are fabricated with electron-beam lithography by defining a gold wire with a 40 nm wide constriction on top of a flexible substrate coated with an insulating layer of polyimide, depicted in Figure 1c. Once fabricated, the sample is mounted in a three-point bending mechanism, clamped between two lateral supports and the head of a central pushing rod, which is connected to a cantilever that is driven either by a stepper motor or a piezoelectric element. Upon bending, the gold wire stretches until its rupture, which leaves two atomically sharp electrodes whose separation can be adjusted mechanically. The ratio between the vertical displacement of the pushing rod and the distance change between the electrodes is 5×10^{-5}, resulting in picometre control over the electrode separation. By unbending the substrate, the two broken extremities fuse to create a continuous wire. This bending-unbending process can be repeated thousands of times without a noticeable aging of the wire.

At room temperature, an MCBJ experiment starts with the characterization of the clean gold electrodes by measuring the low-bias (0.1 V) conductance while breaking and reforming the wire. During the breaking event, a transition occurs from ballistic conduction through few-atom gold contacts (conductance $\geq 1\ G_0 \approx 77\ \mu S$, $G_0 = 2e^2/h$) to a tunneling regime across the broken wire (conductance $\ll 1\ G_0$) either in air or vacuum. The quantum of conductance G_0 defines the conductance of a quantum channel for a unitary transmission probability of electrons passing through it and corresponds also to the largest conductance that can be reached in a quantum object (such as a single molecule).

The distance dependence of the current in the ballistic and tunneling regimes is very different, showing steps and flat plateaus in the former case and an exponential decay in the latter. If instead a molecule bridges the two electrodes and hybridizes with both of them, electrons can tunnel through the molecular orbitals and the distance dependence of the conductance typically shows plateaus and steps. In the case of

DOI: 10.1021/acs.accounts.7b00493
Acc. Chem. Res. 2018, 51, 1359−1367

OPE3, the conductance is dominated by the frontier orbitals depicted in Figure 1d. On the bare junction, we measure typically a few thousand conductance-displacement traces to check for the presence of contaminants in the device and to extract the calibration factor of the electrode displacement by using the length of single-gold atom plateaus in these traces (Figure S2).[24,25]

III. ROOM-TEMPERATURE MEASUREMENTS

Deposition of OPE3 molecules is done by pipeting onto the MCBJ device a 1 μL droplet of a 1 mmol/L solution in dichloromethane with the addition of 2 equiv of tetrabutylammonium hydroxide, which deprotects the thiol groups favoring the formation of gold−sulfur bonds.[16,26] During the deposition of the molecular solution, we monitor the conductance while breaking and reforming the electrodes. In the case of OPE3, the formation of single-molecule contacts starts as soon as the molecular solution is deposited onto the electrodes and plateaus in the conductance versus electrode spacing traces are a sign of their formation. Figure 2a displays such a conductance trace with a clear plateau that is 1 nm long and centered around 10^{-4} G_0.

A conductance histogram built from the trace in panel (a) is shown in Figure 2b. The peak in the histogram centered around 10^{-4} G_0 corresponds to the conductance of the molecular junction and the peak width reflects the variability in the conformations and/or in the local environment felt by the molecule. A different representation of the same histogram is also shown, in which the counts of the histogram are represented as colors. Figure 2c represents a full data set built up from 1450 consecutive breaking traces measured as a function of time starting from the deposition of the molecular solution. With an electrode displacement speed of 5 nm/s, each breaking trace takes between 3 and 6 s. The 2D histogram reveals that the measurements are homogeneous in time apart from the first 100 traces in which mostly empty junctions appear. Moreover, the diagram shows that even after the initial 100 traces, not all traces contain molecular features.

A junction formation yield as high as possible is not desirable in single-molecule experiments. In fact, the larger the yield, the larger the probability that more than one molecule bridges the gap between the electrodes, either in series (dimerization) or in parallel (clusterization). In these cases, it is more difficult to disentangle single-molecule properties from the measurements; for example, in the conductance histograms, additional structures may appear connected with the formation of junctions with two molecules in parallel.[27] Yield rates of 10−30% are usual, and yield rates of 90% or more are not advisible. We further note that yield variations occur when comparing different MCBJ samples and/or molecules despite keeping the experimental conditions the same. One important aspect in the junction formation is that molecules have to diffuse inside the gap; temperature, density of molecules adsorbed, gold-molecule interactions, and contact geometry are key aspects in determining this process and thus the junction-formation yield.

A final comment concerns the use of breaking traces and the disregard of making traces. While in the breaking, atomically sharp tips are formed that face each other as evidenced in 1D and 2D conductance histograms by a clear feature at 1 G_0; in the making of the junction, one cannot be sure that this is the case since the contacts may reconfigure and the two closest points may not face each other, further complicating the analysis of the data. Moreover, the electrode snap-back effect happening at the jump-out-of-contact, which separates the metallic ballistic region from the tunnelling one setting the origin of the displacement scale, is only clearly present during the breaking. The electrodes, right after the breaking, are spaced apart by a certain distance that in previous studies was estimated to be about 0.5 nm.[24]

Functions commonly used for statistical analysis of single-molecule data sets assume stochasticity of the data, i.e., each single-molecule junction is independent from the other ones meaning that each open−close cycle can be considered as a separate experiment. This can be achieved experimentally by forming a new electrode configuration for every cycle. To enforce that, at the end of every breaking trace, we push the electrodes back to a state in which a continuous wire with substantial thickness has been recreated by imposing that it has a conductance of 30−40 G_0, corresponding to a diameter of few nanometers.

To check that this intuitive picture indeed leads to independent rupture events, we analyze the separation between the successful formation of molecular junctions. This problem can be modeled by picturing the junction opening as the flip of a (biased) coin, the capturing of a molecule as a head (win) and an empty junction as a tail (loss). In other words, the process is a series of Bernoullli trials. This means that the distribution of the separation between two consecutive molecular junctions should follow the geometric distribution:

$$P(n) = (1 - p)^{n-1}p \tag{1}$$

where n is the number of breaking traces recorded after trapping of a molecule and p is the overall yield rate of the experiment. If capturing a molecule is a random event, the experimental separation between molecular junctions follows this geometric distribution. As illustrated in Figure 2d, this is indeed the case for the conditions used in our experiment.

Individual conductance versus length traces are typically collected in 1D and 2D histograms. To determine the molecular-junction formation yield, one has to distinguish between molecular and empty junctions. With recent technical advances, the acquisition of data sets exceeding tens of thousands of breaking traces is common and we developed a simple method for selecting molecular junctions.

The conductance of breaking traces of empty junctions shows an exponential decay with increasing displacement, but if a molecule is trapped the conductance remains higher at larger electrode displacements. Exploiting this fact we sum all counts recorded between 1×10^{-2} G_0 and 1×10^{-5} G_0 and label as molecular ones those that have more counts in that region than the average; 1D and 2D histograms are then built (Figure 3). This procedure can help uncover features due to molecular configurations that would otherwise be hidden by other more probable configurations. For example, in Figure 3b, a short region of higher counts is visible above the main high-count conductance region. This higher conductance feature is present in other devices as well.

In this Account, we discuss in detail the results of two devices measured at room temperature and two at cryogenic temperatures. Samples measured at low temperatures are typically not used for room-temperature measurements and vice versa since the technical requirements of the measuring setups are different. In the SI we discuss five additional room-temperature devices. The measurements−done over the course of several years- were performed with the same molecular concentration and with the same experimental settings. Table S1 summarizes

DOI: 10.1021/acs.accounts.7b00493
Acc. Chem. Res. 2018, 51, 1359−1367

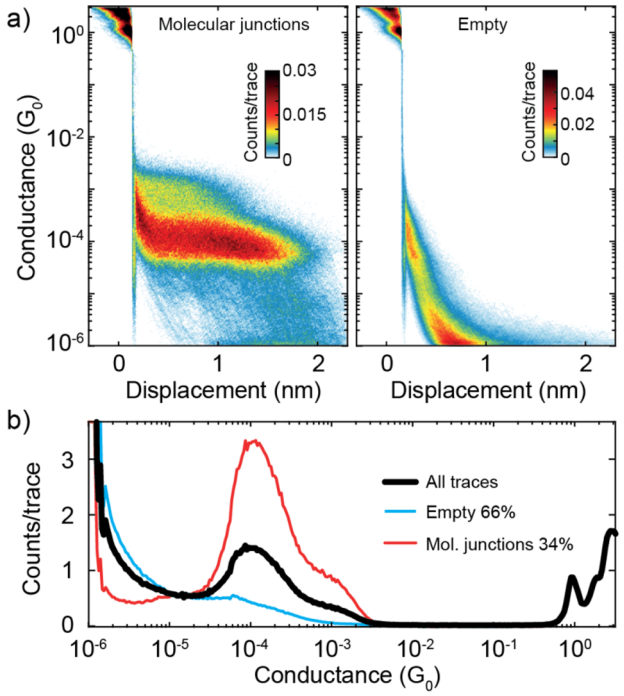

Figure 3. (a) 2D conductance-displacement histograms of OPE3 built from 10 000 breaking traces (bias 0.1 V and speed 4.5 nm/s. The curves in each histogram have been automatically filtered as described in the main text and correspond to molecular junctions (left) and empty tunnel traces (right). (b) Conductance histograms built from all traces (black thick line) and from the two automatically selected groups (thin lines).

some of the important parameters obtained from the histograms: the most probable conductance as determined from a fit to the peak representing the molecules in the full data set and in the filtered 1D histogram, the full-width at half-maximum of this peak, the average plateau length and the junction yield.

As the table shows, variations in the parameters are observed. The most probable conductance value ranges from 1 to 2.4 × 10^{-4} G_0, about a factor two of difference. The full width half-maximum is about 1 order of magnitude in conductance for all cases. The average plateau length ranges from 0.9 to 1.5 nm. Finally, the sample yield at room temperature changes by an order of magnitude from 7% to 75% among the seven samples. The junction yield thus seems to be determined by geometrical and concentration differences in the region close to the separated electrodes, as the other parameters that may influence it are held the same.

To access the stability of the molecule-electrode interfaces and how the mechanical stability depends on the anchoring groups, we have recorded conductance-time traces with the self-breaking technique.[20] In this experiment the gold wire is stretched until the low-bias conductance reaches a value of $10G_0$. Subsequently, a bias voltage of 0.1 V is applied and the current flowing through the wire is measured. Due to the built-up strain, the Au wire spontaneously breaks (self-breaking) while the conductance is measured as a function of time. Once the conductance falls below 2 × 10^{-7} G_0, the electrodes are fused again until the conductance reaches $40G_0$. The sequence is then repeated and hundreds of traces can be collected.

Figure 4 shows examples of conductance-time traces measured on OPE3 in a fast-breaking experiment (Figure 4a) and in the self-breaking regime with the electrodes stopped as described above (Figure 4b). Remarkably, we find that the lifetime of the molecular junctions formed with the self-breaking method can reach thousands of seconds (the lifetime of empty junctions is a few seconds at most). Figure 4c shows the conductance histograms of OPE3 built from self-breaking traces (thick line) and from fast breaking traces (thin line). The self-breaking histogram displays a sharp peak centered around 10^{-3} G_0, which is a value comparable to the high-conductance shoulder observed in the fast breaking histogram of OPE3. This configuration appears to be more stable than the one with a conductance around 10^{-4} G_0 which is the one observed more often in the fast breaking experiments and probably involves the overlap of the outer phenyl rings with the gold electrodes, providing an additional mechanical anchor.

The stability of the MCBJ technique allows one to measure current (I) versus bias voltage (V) characteristics at different electrode separations. A simplified model can be used to extract the level alignment and the electronic metal-molecule coupling from the data.[28−30] Since thousands of I−V's can be recorded during different breaking traces, a statistical analysis can be adopted to analyze the results.

To measure current−voltage characteristics of molecular junctions we separate the electrodes at a lower speed than during the acquisition of the conductance traces discussed above, typically at a speed of 0.01 nm/s. While the gold wire is still intact, the bias is swept between −0.1 and 0.1 V until the

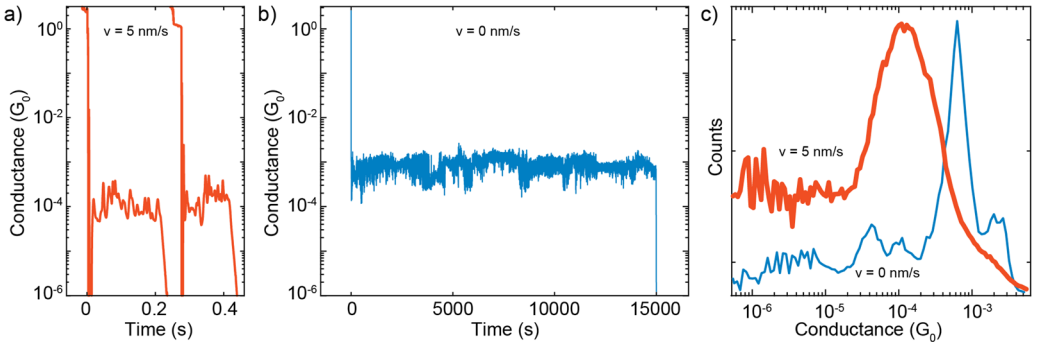

Figure 4. (a) Individual breaking traces measured in the presence of OPE3 molecules (bias 0.1 V and speed 5 nm/s). The traces are offset along the x-axis for clarity. (b) Same as (a) with the electrodes stopped. (c) Conductance histograms built from the conductance traces recorded in the presence of the molecule. The red thick curve is the histogram built from 1450 fast breaking traces (v = 5 nm/s), and the blue thin line is built from 275 self-breaking traces (v = 0 nm/s). Adapted with permission from ref 20. Copyright Beilstein-Institut.

DOI: 10.1021/acs.accounts.7b00493
Acc. Chem. Res. 2018, 51, 1359−1367

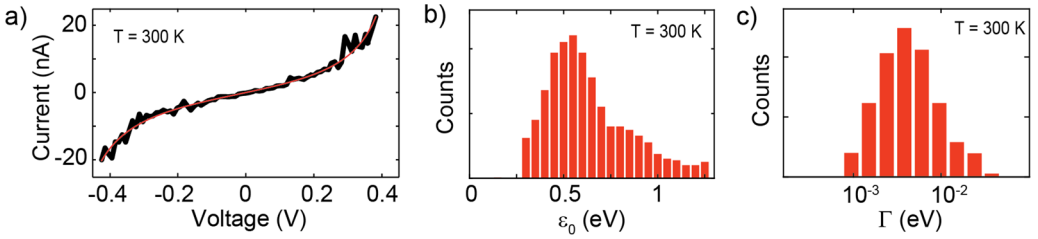

Figure 5. (a) An example of a room temperature $I-V$ of OPE3. The black thick line represents the experimental data while the red thin curve is a fit to the single-level model. (b,c) Parameters extracted from the fit of 985 room temperature $I-V$'s.

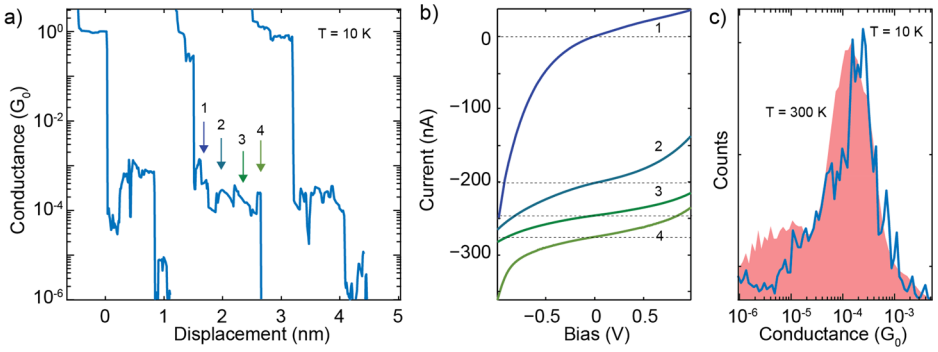

Figure 6. (a) Breaking traces, recorded in the presence of OPE3 (sample 3) at a temperature of 10 K (bias 0.1 V). The traces have been offset along the x-axis for clarity. (b) Current−voltage characteristics measured during the central breaking trace shown in (a), shifted along the y-axis for clarity. (c) Conductance histogram built from molecular low temperature and room temperature conductance traces. Adapted with permission from ref 22. Copyright American Physical Society.

low-bias conductance reaches a value smaller than $0.1G_0$. After this, we continuously sweep the voltage between −0.7 and 0.7 V at a rate of 0.05 V/s. At room temperature the voltage applied to a single-molecule junction cannot be too high and empirically the value of 0.8 V appears to be the maximum. On the other hand, at low temperatures, higher voltages up to a few volts can be applied. Once the low-bias conductance drops below $10^{-6}G_0$, the gold contact is reformed until the conductance reaches $30-40G_0$ and a new breaking trace starts. In this way, hundreds of individual $I-V$ breaking traces are recorded yielding thousands of individual I-Vs.

The asymmetric Breit−Wigner model[31,32] can be used to extract quantitative information from the $I-V$'s yielding three parameters: the electronic coupling between molecule and left and right electrode, respectively Γ_L and Γ_R, and the injection barrier ε_0, defined as the misalignment between the Fermi energy of the electrodes (E_F) and the energy of the closest frontier orbital $\varepsilon_0 = |E_F - \varepsilon|$, where ε is the energy of the closest frontier molecular orbital. In the Landauer transport formalism,[33] the current is given by

$$I(V) = \int_{E_F - eV/2}^{E_F + eV/2} T(E)\, dE \qquad (2)$$

where $T(E)$ is the transmission, which in the single-level model is a Lorentzian peak centered at ε_0 and broadened by the electronic coupling $\Gamma = \Gamma_L + \Gamma_R$. An asymmetry in the $I-V$ can be modeled by introducing a voltage dependence in the Lorentzian peak position, that is, replacing ε_0 with $\varepsilon_0(V) = \varepsilon_0 + \eta V/2$, where η is a dimensionless parameter between −1 and 1 ($\eta = 0$ gives symmetric $I-V$'s). Often the approximation $\eta = (\Gamma_L - \Gamma_R)/(\Gamma_L + \Gamma_R)$ is used, but one should keep in mind that η depends on the capacitive coupling, which in principle is independent from the asymmetry in the resistance coupling.

In Figure 5a, the drawn red line is a fit of a measured $I-V$ characteristic to the single-level model. Good agreement is found with $\varepsilon_0 = 0.49$ eV and $\Gamma = 9$ meV. Note that in this case a symmetric bias was chosen so that $\eta = 0$. The fitting has been performed on 985 $I-V$'s obtained from 40 different molecular junctions. Figure 5b,c shows the histograms of the fit parameters: the level alignment peaks around 0.5 eV with a long tail toward energies up to 1.5 eV. The electronic coupling ranges from 1 to 20 meV; the average value is 8 meV. It is important to realize that these results depend on the anchoring group, which indicates the importance of charge redistributions near the interface, which affect the electrostatic environment of the molecule and thereby its level alignment.

IV. LOW-TEMPERATURE MEASUREMENTS

When carrying out MCBJ measurements at cryogenic temperatures, a stepper motor connected to a differential screw is used instead of a piezo. The electrode speed is limited to 0.2 nm/s and thus a longer measurement time is needed to complete each breaking event. Moreover, due to the reduced atomic and molecular mobility at low temperature, the molecular junction formation yield is strongly reduced, going from approximately 10−70% at room temperature to 2−5% at low temperatures. The combination of a longer measuring time and lower junction formation yield implies that a smaller number of molecular junctions can be probed as compared to room-temperature studies. The main advantages at low temperature, on the other hand, are the reduced thermal noise, which allows for more precise electrical measurements, and the increased electrode and molecule−electrode stability, that permits larger bias voltages to be applied.

Figure 6a displays three conductance versus displacement traces measured on OPE3 at a temperature of 10 K. In the region below 1 G_0, the conductance traces show plateaus,

DOI: 10.1021/acs.accounts.7b00493
Acc. Chem. Res. 2018, 51, 1359−1367

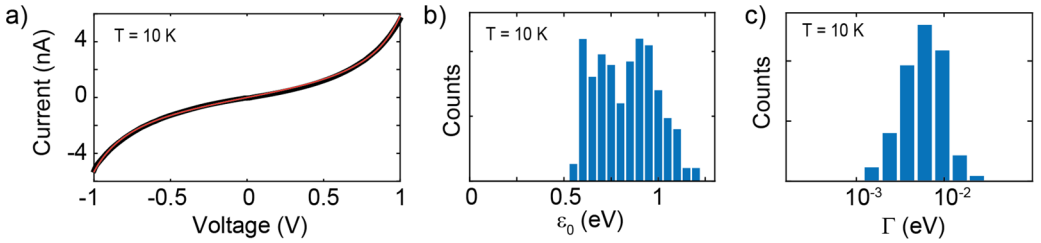

Figure 7. (a) Example of a low-temperature $I-V$ of OPE3. The black thick line represents the experimental data, while the red thin curve is a fit to the single-level model. (b,c) Parameters extracted from the fit of 297 low temperature $I-V$'s.

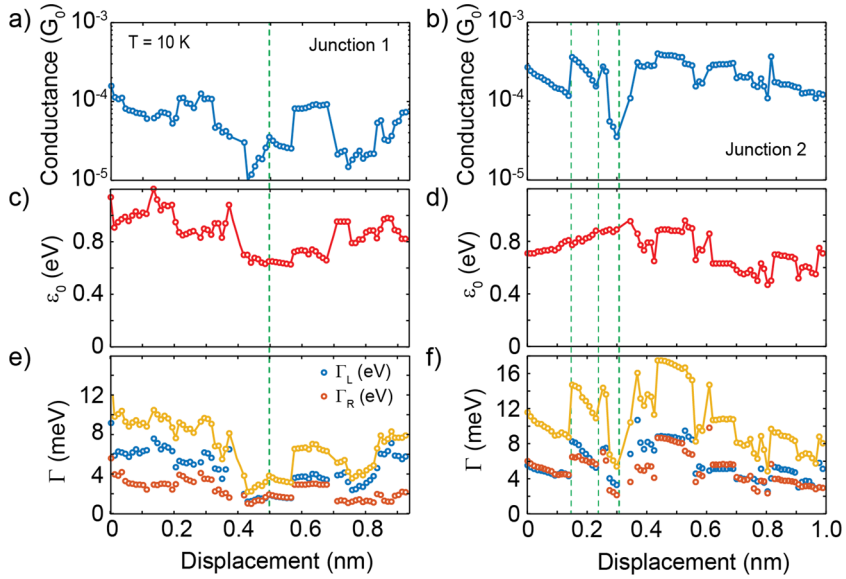

Figure 8. (a,b) Low-temperature conductance traces obtained from a low-bias fit of $I-V$'s. (c,d) Corresponding level alignment and (e,f) electronic coupling during electrode separation as determined from fits to the Breit–Wigner model.

typically at around 10^{-4} G_0, a value similar to the room-temperature one. The plateaus extend for a length of about 1.5 nm after which the conductance drops to the noise level of the setup. The three plateaus present regions in which the conductance evolves gradually and regions with abrupt conductance changes. We have measured more than 1000 breaking traces and built a conductance histogram, shown in Figure 6b, by selecting the 38 traces that show a conductance plateau in the region between 10^{-2} G_0 and 10^{-5} G_0 with the filter procedure discussed earlier (junction formation probability of 3.5%). The low-temperature conductance histogram can be compared to the room-temperature one. Apart from the better signal-to-noise ratio in the latter histogram, the distribution of conductance values is similar; at both temperatures the conductance peak has a width of approximately 1 order of magnitude and is centered respectively around 1.8×10^{-4} G_0 (10 K) and $1.2 \times 10^{-4} G_0$ (300 K). These observations support coherent tunneling as the main transport mechanism in single-OPE3 junctions.

During a low-temperature breaking trace one can also record $I-V$'s at each electrode position (with minimum separation being approximately 10 pm). Figure 6c shows four $I-V$'s measured at four different positions in the central breaking trace displayed in Figure 6a. The current can be asymmetric in voltage (I-Vs 1,4) or symmetric ($I-V$'s 2,3) and conductance switches, either gradually or abruptly, occur while stretching. Configurational noise, which at room temperature manifests itself in a large width of molecular conductance peaks, translates at low temperature into clear jumps. Interestingly, $I-V$'s recorded just after molecular-junction formation typically present a large asymmetry; the coupling to the electrodes being is in this case very asymmetric. A possible scenario involves the interaction of only one phenyl ring with one electrode, while on the other side a sulfur–gold connection provides the coupling.

Figure 7a shows one $I-V$ characteristic of a molecular junction recorded in the central breaking trace of Figure 6a (plateau region). The $I-V$ is symmetric, and it can be well fitted to the Breit–Wigner model with parameters $\varepsilon_0 = 0.64$ eV and $\Gamma_L = \Gamma_R = 0.3$ meV. We fitted 297 $I-V$'s recorded from 13 breaking traces showing molecular plateaus and collected the fit parameters in the histograms of Figure 7b,c. Similarly to the room temperature case, a parameter spread is observed as evidenced in the histogram widths. The level alignment is shifted to slightly larger values compared to the room temperature case, whereas the electronic coupling covers the range from 1 to 10 meV.

The high junction stability at low temperature allows following the evolution of the fit parameters upon separating the electrodes. Figure 8a,b displays two conductance plateaus with a conductance that fluctuates around $5 \times 10^{-5} G_0$ and around $2 \times 10^{-4} G_0$ respectively, with continuous regions (in which the conductance gradually increases or decreases) separated by abrupt jumps. Figure 8c,d shows the level alignment at each position for the two junctions, while Figure 8e,f shows the electronic coupling. In the continuous regions,

DOI: 10.1021/acs.accounts.7b00493
Acc. Chem. Res. 2018, 51, 1359–1367

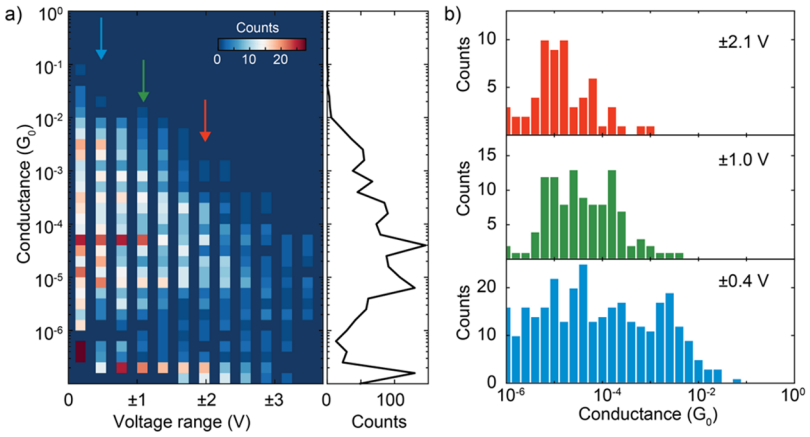

Figure 9. (a) Histogram of the zero-bias conductance versus the voltage limit of the $I-V$ (at cryogenics temperature of ≈6 K). Red points have high counts, while blue ones have low counts. The inset shows the conductance distribution obtained by integrating over the voltage range. (b) Low-bias conductance distribution of an $I-V$ recorded to a given voltage limit. The histograms are built from $I-V$'s with ±0.4 V voltage sweep (blue), ± 1.0 V (green), and ±2.1 V (red).

the parameters ε_0, Γ_L, and Γ_R gradually change value. In contrast, conductance jumps induce abrupt changes either in the coupling or in the level alignment or in both parameters at the same time. In junction 2 in Figure 8b, one can see that in the first part of the stretching both the conductance and the electronic coupling show three jumps while the level alignment evolves gradually from 0.7 to 0.95 eV at 0.8 eV/nm. The measurements thus confirm the intuitive picture that the jumps are connected to abrupt changes in the junction conformation at the atomic level.

We have also investigated the $I-V$'s when exposed to bias voltages up to 3.7 V at cryogenic temperature (≈6 K). The measurements initially follow the standard procedure of stretching the gold wire until it ruptures, forming the electrodes. The conductance is measured continuously during this process, until the drop in conductance signals the opening of the junction. At this point, the electrodes are displaced further by 0.4 nm and then an $I-V$ curve is recorded. In the first $I-V$, the voltage is swept in the range of ±0.1 V. After this displacement of 0.4 nm, empty junctions have a conductance lower than the noise level (10^{-7} G_0), while for molecular junctions the conductance remains well above this level and in this case another $I-V$ is taken with a voltage sweep that is larger by a value of 0.3 V. The process is repeated until the zero-bias conductance falls below 10^{-7} G_0 or until a voltage limit of ±3.7 V is reached.

Figure 9a shows the distribution of the zero-bias conductance values obtained from the $I-V$'s versus the maximum voltage applied before losing the molecule. Blue areas represent low counts, while red areas indicate high counts. The inset shows the corresponding 1D conductance histogram, which indicates that more than one conductance value can be found. The most probable conductance at room temperature (1.5×10^{-4} G_0) is one of the values, but not the most likely one in this type of measurement. A large percentage of I-Vs has conductance values centered around 10^{-3} G_0 and 10^{-5} G_0. The presence of different conductance values is due to the different junction configurations which are stable at low temperature.

Figure 9b shows the conductance histogram for $I-V$'s with the same voltage limit. Going from ±0.4 V (blue histogram) to ±1.0 V (green) and ±2.1 V (red), an overall decrease of counts at high conductance values is observed while peaks at lower conductance become more relevant. The counts around 10^{-3} G_0 are prominent at ±0.4 V, but decrease considerably at ±1.0 V and are absent for junctions to which more than ±2.1 V has been applied. A similar behavior is observed for the $I-V$'s with a conductance of 10^{-4} G_0, which make up the majority of conductance values up to ±1.0 V but decrease sharply in numbers for larger voltages allowing the conductance values around 10^{-5} G_0 to become the most probable ones in that region. The choice of the bias voltage range can thus change dramatically the single-molecule conductance distribution.

V. CONCLUDING REMARKS

We presented a detailed study of the transport properties of single OPE3 molecules anchored to gold electrodes. Different experimental protocols yield different information about the molecular behavior, providing a consistent and extended picture of the variability that is omnipresent in single-molecule studies. The measurements show that a single molecule can be contacted by two metal electrodes, but the atomistic configuration of each single junction is not known. Statistics helps to understand the overall behavior from which a clear picture of the average configuration emerges. This picture is solely based on the information obtained from electrical characteristics, and it would therefore be beneficial to directly link the experimental data to theoretical calculations, which should then take the microscopic variability into account. As such, the results presented in this Account could form a starting point to initiate more statistical studies on the formation and evolution of molecular junctions and how the different configurations affect their electrical properties.

■ ASSOCIATED CONTENT

Supporting Information

The Supporting Information is available free of charge on the ACS Publications website at DOI: 10.1021/acs.accounts.7b00493.

Details on the pristine MCBJ sample characterization, histogram filtering method and high-bias, low-temperature experiment (PDF)

DOI: 10.1021/acs.accounts.7b00493
Acc. Chem. Res. 2018, 51, 1359−1367

AUTHOR INFORMATION

Corresponding Authors

*E-mail: riccardo.frisenda@imdea.org.
*E-mail: h.s.j.vanderzant@tudelft.nl.

ORCID

Riccardo Frisenda: 0000-0003-1728-7354
Davide Stefani: 0000-0002-9406-9265

Author Contributions

[‖]R.F. and D.S. contributed equally to this work.

Notes

The authors declare no competing financial interest.

Biographies

Dr. Riccardo Frisenda earned his Ph.D. in 2016 at the Technical University of Delft in the Netherlands. He then won a Rubicon grant and has been working at IMDEA Nanoscience, Madrid as a postdoctoral fellow studying optoelectronic properties of two-dimensional materials.

Davide Stefani is a Ph.D. student at the Technical University of Delft in The Netherlands, where he investigates single-molecule transport.

Prof. Dr. Herre S. J. van der Zant is a full professor at the Kavli Institute of Nanoscience at the Technical University of Delft in The Netherlands. He studies nanoelectronics and nanomechanics with a focus on single-molecule transport.

ACKNOWLEDGMENTS

This work was financially supported by The Netherlands Organisation for Scientific Research (NWO), the European Union's Seventh Framework Programme (FP7/2007-2013), ERC Advanced Grant agreement number 240299 (Mols@Mols). R.F. acknowledges support from NWO through a Rubicon grant (680-50-1515).

REFERENCES

(1) Nitzan, A.; Ratner, M. A. Electron transport in molecular wire junctions. *Science* **2003**, *300*, 1384−1389.
(2) Aradhya, S. V.; Venkataraman, L. Single-molecule junctions beyond electronic transport. *Nat. Nanotechnol.* **2013**, *8*, 399−410.
(3) Xiang, D.; Wang, X.; Jia, C.; Lee, T.; Guo, X. Molecular-scale electronics: from concept to function. *Chem. Rev.* **2016**, *116*, 4318−4440.
(4) Hybertsen, M. S.; Venkataraman, L. Structure−property relationships in atomic-scale junctions: Histograms and beyond. *Acc. Chem. Res.* **2016**, *49*, 452−460.
(5) Su, T. A.; Li, H.; Klausen, R. S.; Kim, N. T.; Neupane, M.; Leighton, J. L.; Steigerwald, M. L.; Venkataraman, L.; Nuckolls, C. Silane and Germane Molecular Electronics. *Acc. Chem. Res.* **2017**, *50*, 1088−1095.
(6) Xu, B.; Tao, N. J. Measurement of single-molecule resistance by repeated formation of molecular junctions. *Science* **2003**, *301*, 1221−1223.
(7) Naidyuk, Y. G.; Yanson, I. K. *Point-contact spectroscopy*; Springer Science & Business Media: 2005; Vol. *145*.
(8) Konishi, T.; Kiguchi, M.; Takase, M.; Nagasawa, F.; Nabika, H.; Ikeda, K.; Uosaki, K.; Ueno, K.; Misawa, H.; Murakoshi, K. Single Molecule Dynamics at a Mechanically Controllable Break Junction in Solution at Room Temperature. *J. Am. Chem. Soc.* **2013**, *135*, 1009−1014.
(9) Parker, C. R.; Leary, E.; Frisenda, R.; Wei, Z.; Jennum, K. S.; Glibstrup, E.; Abrahamsen, P. B.; Santella, M.; Christensen, M. A.; Della Pia, E. A.; Li, T.; Gonzalez, M. T.; Jiang, X.; Morsing, T. J.; Rubio-Bollinger, G.; Laursen, B. W.; Nørgaard, K.; van der Zant, H.; Agrait, N.; Nielsen, M. B. A Comprehensive Study of Extended Tetrathiafulvalene Cruciform Molecules for Molecular Electronics: Synthesis and Electrical Transport Measurements. *J. Am. Chem. Soc.* **2014**, *136*, 16497−16507.
(10) Kim, T.; Darancet, P.; Widawsky, J. R.; Kotiuga, M.; Quek, S. Y.; Neaton, J. B.; Venkataraman, L. Determination of Energy Level Alignment and Coupling Strength in 4,4′-Bipyridine Single-Molecule Junctions. *Nano Lett.* **2014**, *14*, 794−798.
(11) Donhauser, Z. J.; Mantooth, B. A.; Kelly, K. F.; Bumm, L. A.; Monnell, J. D.; Stapleton, J. J.; Price, D. W., Jr; Rawlett, A. M.; Allara, D. L.; Tour, J. M.; Weiss, P. S. Conductance switching in single molecules through conformational changes. *Science* **2001**, *292*, 2303−2307.
(12) Mayor, M.; Weber, H. B.; Reichert, J.; Elbing, M.; von Hanisch, C.; Beckmann, D.; Fischer, M. Electric current through a molecular rod - Relevance of the position of the anchor groups. *Angew. Chem., Int. Ed.* **2003**, *42*, 5834−5838.
(13) Kubatkin, S.; Danilov, A.; Hjort, M.; Cornil, J.; Brédas, J.-L.; Stuhr-Hansen, N.; Hedegård, P.; Bjørnholm, T. Single electron transistor with a single conjugated molecule. *Curr. Appl. Phys.* **2004**, *4*, 554−558.
(14) Wu, S.; Gonzalez, M. T.; Huber, R.; Grunder, S.; Mayor, M.; Schonenberger, C.; Calame, M. Molecular junctions based on aromatic coupling. *Nat. Nanotechnol.* **2008**, *3*, 569−74.
(15) Huber, R.; Gonzalez, M. T.; Wu, S.; Langer, M.; Grunder, S.; Horhoiu, V.; Mayor, M.; Bryce, M. R.; Wang, C. S.; Jitchati, R.; Schonenberger, C.; Calame, M. Electrical conductance of conjugated oligomers at the single molecule level. *J. Am. Chem. Soc.* **2008**, *130*, 1080−1084.
(16) Gonzalez, M. T.; Leary, E.; Garcia, R.; Verma, P.; Herranz, M. A.; Rubio-Bollinger, G.; Martin, N.; Agrait, N. Break-Junction Experiments on Acetyl-Protected Conjugated Dithiols under Different Environmental Conditions. *J. Phys. Chem. C* **2011**, *115*, 17973−17978.
(17) Kaliginedi, V.; Moreno-Garcia, P.; Valkenier, H.; Hong, W. J.; Garcia-Suarez, V. M.; Buiter, P.; Otten, J. L. H.; Hummelen, J. C.; Lambert, C. J.; Wandlowski, T. Correlations between Molecular Structure and Single-Junction Conductance: A Case Study with Oligo(phenylene-ethynylene)-Type Wires. *J. Am. Chem. Soc.* **2012**, *134*, 5262−5275.
(18) Frisenda, R.; Perrin, M. L.; Valkenier, H.; Hummelen, J. C.; van der Zant, H. S. J. Statistical analysis of single-molecule breaking traces. *Phys. Status Solidi B* **2013**, *250*, 2431−2436.
(19) Parker, C. R.; Leary, E.; Frisenda, R.; Wei, Z.; Jennum, K. S.; Glibstrup, E.; Abrahamsen, P. B.; Santella, M.; Christensen, M. A.; Della Pia, E. A.; Li, T.; Gonzalez, M. T.; Jiang, X.; Morsing, T. J.; Rubio-Bollinger, G.; Laursen, B. W.; Norgaard, K.; van der Zant, H.; Agrait, N.; Nielsen, M. B. A comprehensive study of extended tetrathiafulvalene cruciform molecules for molecular electronics: synthesis and electrical transport measurements. *J. Am. Chem. Soc.* **2014**, *136*, 16497−507.
(20) Frisenda, R.; Tarkuç, S.; Galán, E.; Perrin, M. L.; Eelkema, R.; Grozema, F. C.; van der Zant, H. S. J. Electrical properties and mechanical stability of anchoring groups for single-molecule electronics. *Beilstein J. Nanotechnol.* **2015**, *6*, 1558−1567.
(21) Frisenda, R.; Perrin, M. L.; van der Zant, H. S. Probing the local environment of a single OPE3 molecule using inelastic tunneling electron spectroscopy. *Beilstein J. Nanotechnol.* **2015**, *6*, 2477.
(22) Frisenda, R.; van der Zant, H. Transition from Strong to Weak Electronic Coupling in a Single-Molecule Junction. *Phys. Rev. Lett.* **2016**, *117*, 126804.
(23) Frisenda, R.; Janssen, V. A.; Grozema, F. C.; van der Zant, H. S.; Renaud, N. Mechanically controlled quantum interference in individual π-stacked dimers. *Nat. Chem.* **2016**, *8*, 1099.
(24) Untiedt, C.; Yanson, A. I.; Grande, R.; Rubio-Bollinger, G.; Agraït, N.; Vieira, S.; van Ruitenbeek, J. M. Calibration of the length of a chain of single gold atoms. *Phys. Rev. B: Condens. Matter Mater. Phys.* **2002**, *66*, 085418.

DOI: 10.1021/acs.accounts.7b00493
Acc. Chem. Res. 2018, 51, 1359−1367

(25) Yanson, A. I.; Bollinger, G. R.; van den Brom, H. E.; Agrait, N.; van Ruitenbeek, J. M. Formation and manipulation of a metallic wire of single gold atoms. *Nature* **1998**, *395*, 783−785.
(26) Valkenier, H.; Huisman, E. H.; van Hal, P. A.; de Leeuw, D. M.; Chiechi, R. C.; Hummelen, J. C. Formation of high-quality self-assembled monolayers of conjugated dithiols on gold: base matters. *J. Am. Chem. Soc.* **2011**, *133*, 4930−9.
(27) Reuter, M. G.; Hersam, M. C.; Seideman, T.; Ratner, M. A. Signatures of Cooperative Effects and Transport Mechanisms in Conductance Histograms. *Nano Lett.* **2012**, *12*, 2243−2248.
(28) Xie, Z.; Baldea, I.; Smith, C. E.; Wu, Y.; Frisbie, C. D. Experimental and Theoretical Analysis of Nanotransport in Oligophenylene Dithiol Junctions as a Function of Molecular Length and Contact Work Function. *ACS Nano* **2015**, *9*, 8022−36.
(29) Kim, Y.; Hellmuth, T. J.; Sysoiev, D.; Pauly, F.; Pietsch, T.; Wolf, J.; Erbe, A.; Huhn, T.; Groth, U.; Steiner, U. E.; Scheer, E. Charge Transport Characteristics of Diarylethene Photoswitching Single-Molecule Junctions. *Nano Lett.* **2012**, *12*, 3736−3742.
(30) Zotti, L. A.; Kirchner, T.; Cuevas, J. C.; Pauly, F.; Huhn, T.; Scheer, E.; Erbe, A. Revealing the Role of Anchoring Groups in the Electrical Conduction Through Single-Molecule Junctions. *Small* **2010**, *6*, 1529−1535.
(31) Xue, Y.; Datta, S.; Ratner, M. A. First-principles based matrix Green's function approach to molecular electronic devices: general formalism. *Chem. Phys.* **2002**, *281*, 151−170.
(32) Cuevas, J. C., Scheer, E., Eds. *Molecular electronics: An introduction to theory and experiment*; World Scientific: 2010; Vol. *1*, DOI: 10.1142/7434.
(33) Imry, Y.; Landauer, R. Conductance viewed as transmission. *Rev. Mod. Phys.* **1999**, *71*, S306−S312.

DOI: 10.1021/acs.accounts.7b00493
Acc. Chem. Res. 2018, 51, 1359−1367